

Calculations of anisotropic magnetic properties using spin-orbit energy variations

C. Liu , Y. X. Yao , C.-Z. Wang, K.-M. Ho, and V. P. Antropov

Ames Laboratory, U.S. DOE and Department of Physics and Astronomy, Iowa State University, Ames, Iowa 50011, USA

 (Received 8 September 2020; revised 2 November 2020; accepted 3 November 2020; published 19 November 2020)

We analyze several methods of obtaining the accurate relativistic total energy (TE) variations using traditional perturbation theories (PTs) and proposed coupling constant integration (CCI) methods. For this purpose, we perform benchmark calculations within the density functional theory taking the spin-orbit coupling (SOC) and its derivative as a perturbation. The TE change due to SOC addition obtained from both PTs and CCI is shown to reach the accuracy of fully self-consistent TE calculations. Similar accuracy is also obtained even for the magnetocrystalline anisotropy energy (MAE). The real advantage of the proposed methods is to use PTs and CCI methods in those electronic structure methods where accurate total energies currently cannot be obtained with required accuracy. Correspondingly, we demonstrate the applicability of suggested methods for calculations of MAE in different magnetic materials using a dynamic mean-field method. All suggested PTs and CCI methods also provide convenient site, orbital, and spin decompositions of the TE variation, creating a powerful way to analyze microscopic physics in strongly correlated materials.

DOI: [10.1103/PhysRevB.102.205119](https://doi.org/10.1103/PhysRevB.102.205119)

I. INTRODUCTION

The theoretical/experimental quest for realistic material simulations often lies in small energy scales. For instance, the magnetocrystalline anisotropy energy (MAE), which is a key material property crucial for applications of permanent magnets [1], often does not exceed on the order of 1 meV/atom. While standard density functional theory (DFT) is based on local density approximation (LDA), other approximated exchange-correlation energy functionals can readily reach this high precision in the total energy (TE) given the mean-field level of approximation; the many-electron correlation effects, ubiquitous in functional materials involving partially filled d -/ f -shell electrons, pose a great challenge to DFT. DFT calculations often yield material MAE which can be orders of magnitude off from experimental values, and sometimes even the sign can be wrong. Hybrid methods that combine DFT with higher-level many-body techniques to explicitly treat electron correlations have been developed [2–5]. LDA+Hubbard U [6–8] and LDA + dynamical mean-field theory (DMFT) [9,10] have been applied to study the strong electron-correlation effects on MAE for some typical magnetic systems. The GW method [11–13] does not always rely on DFT to provide one-electron dispersion and has also been successfully applied to magnetic systems. It is very challenging, however, to achieve highly accurate TE from state-of-the-art methods such as LDA+DMFT and GW.

The purpose of this work is to analyze the usage of several perturbation theories (PTs) and coupling constant integration (CCI) methods to evaluate theoretically challenging physical properties like MAE in advanced theoretical methods such as LDA+DMFT and GW. We notice below that the origin of MAE in all considered systems comes exclusively from spin-orbit coupling (SOC), although the resulting size of the MAE also depends on other terms in the Hamiltonian. SOC is generally a small “perturbation” term, so PTs and CCI

methods are natural approaches to accurately calculate the change in the induced TE variation. However, such smallness is not a requirement for the applicability of CCI methods. CCI methods traditionally have been used in the electronic structure calculations to estimate correlation energies [14]. Applications of CCI to magnetic calculations are very limited, and we are not familiar with any CCI methods applied to relativistic interactions. We should mention that a variation of SOC and its influence on anisotropic properties were studied earlier (see, for instance, Ref. [8]). A generalization of such variation in the case of the fully relativistic Dirac equation was also proposed [15] in which the inverse of the speed of light was used as a variational parameter.

We carry out a detailed benchmark of the reliability of PTs and CCI methods in calculating the TE variation caused by a small perturbation of SOC. We show that both PTs and CCI methods can efficiently produce results with remarkable accuracy when compared with numerically “exact” self-consistent calculations (SCCs). For convenience, a DFT is chosen to be the theoretical framework as a benchmark. Since both PT and CCI are very general approaches, the main conclusion is expected to apply to other levels of theory as well.

We describe both the CCI and PT formalisms in Sec. II. In Sec. III we benchmark the TE calculations on three paramagnetic bulk materials and present results for MAE calculations for two ferromagnetic materials. Section III also shows the site decomposition of the TE and the DMFT calculations of the MAE for several well-known magnetic systems.

II. METHODS

Let us define the system Hamiltonian as

$$\mathcal{H} = \mathcal{H}_0 + V, \quad (1)$$

where \mathcal{H}_0 is the Hamiltonian including scalar relativistic effects and $V = \xi \mathbf{L} \cdot \mathbf{S}$ denotes the SOC component. This component is usually small when compared to the TE of the system. Generally, we can introduce a coupling constant λ and define

$$\mathcal{H}(\lambda) = \mathcal{H}_0 + \lambda V, \quad (2)$$

where λ varies from 0 to 1, which adiabatically connects a system of \mathcal{H}_0 to that of \mathcal{H} . The TE of the system is given by

$$E(\lambda) = \langle \Psi(\lambda) | \mathcal{H}(\lambda) | \Psi(\lambda) \rangle. \quad (3)$$

In particular, $E_0 = E(\lambda = 0)$ gives the total scalar relativistic energy, and $E(\lambda = 1)$ amounts to the total relativistic energy, including SOC. The expectation value of SOC has the following form:

$$E^{\text{so}}(\lambda) = \langle \Psi(\lambda) | \lambda V | \Psi(\lambda) \rangle. \quad (4)$$

According to the Hellmann-Feynman theorem, we can express the derivative of the TE with respect to λ as

$$\begin{aligned} E'(\lambda) &= \langle \Psi(\lambda) | V | \Psi(\lambda) \rangle \\ &= \frac{E^{\text{so}}(\lambda)}{\lambda}. \end{aligned} \quad (5)$$

Therefore, we can calculate the TE $E(\lambda) = E_0 + \Delta E(\lambda)$ using CCI given that E_0 is known with

$$\Delta E(\lambda) = \int_0^\lambda \frac{E^{\text{so}}(\lambda')}{\lambda'} d\lambda'. \quad (6)$$

In other words, the induced TE change due to the addition of SOC, which includes the response of the system kinetic energy and potential energy, can be determined solely by the SOC along the path of the coupling constant λ .

Finally, the MAE, the TE difference between two different magnetization directions (e.g., [100] and [001] for FePt and CoPt alloys), is readily obtained with

$$\begin{aligned} K &= E_{100}(\lambda = 1) - E_{001}(\lambda = 1) \\ &= \int_0^1 \frac{E_{100}^{\text{so}}(\lambda) - E_{001}^{\text{so}}(\lambda)}{\lambda} d\lambda. \end{aligned} \quad (7)$$

The corresponding PT results can be easily obtained from the CCI equation if we write for the PT energy,

$$\Delta E(\lambda) = \sum_{n=0} \lambda^n E_n. \quad (8)$$

Here, E_n is the energy of the consecutive PT expansion. Thus, the SOC energy E^{so} can be written as

$$E^{\text{so}} = \sum_{n=0} n E_n. \quad (9)$$

In the most popular second-order approximation, for instance, the change in the TE is just half of the mean value of the perturbation operator,

$$E_2 = E^{\text{so}}/2. \quad (10)$$

Thus, for tetragonal materials, the TE change in a system induced by SOC is just half of the SOC energy. Correspondingly, in cubic systems, where the PT starts with the

fourth-order terms, the energy change is

$$E_4 = E^{\text{so}}/4. \quad (11)$$

The calculations of MAE in cubic materials are very computationally demanding even in the LDA, so DMFT studies of MAE in such systems currently cannot be performed consistently. For both polar and chiral magnetic noncentrosymmetric systems, there is already a first term of the PT that is nonzero. In this case, a specific antisymmetric exchange (the Dzyaloshinskii-Moriya [DM] interaction) appears. DM interaction favors spin canting of otherwise parallel aligned magnetic moments and thus is a source of weak ferromagnetic behavior in an antiferromagnet (AFM). This interaction is responsible for the appearance of magnetic skyrmions and is crucial for the explanation of magnetoelectric effects in materials such as multiferroics. The tensor of the DM interaction D_{ij} is linear over the SOC constant.

In summary, the calculations of SOC energy can be used directly to obtain the TE for systems with different crystal symmetries. The corresponding order of the first nonzero term of PT is determined by the crystal symmetry. In the general case in which we do not assume any symmetry, the CCI method described above (CCI below) should be used to determine the strength of different terms of general expansion over the speed of light of the relativistic PT.

A standard PT considers the SOC a perturbation with an inverse speed of light as a smallness parameter. We define this scheme below as PT1. However, some isotropic terms (Darwin and mass-velocity corrections) of similar relativistic smallness have been included in the original scalar relativistic Hamiltonian. One can further modify traditional PT and decompose the spin-orbit coupling matrix into anisotropic and isotropic terms. This will further separate the large isotropic parts (>0.1 eV) from the much smaller anisotropic parts (<0.01 eV) within the SOC. In the simplest approximation, such a PT can be built using a finite difference between SOC operators defined for different directions of magnetic fields (the anisotropy operator). For systems with axial symmetry, this can be written as

$$K^{\text{so}} = E_x^{\text{so}} - E_z^{\text{so}} = \langle \Psi | V | \Psi \rangle_x - \langle \Psi | V | \Psi \rangle_z. \quad (12)$$

Here, both matrix elements of the SOC operator in the right part are calculated separately with the different wave functions and Fermi levels, corresponding to different magnetic field directions. To extract the anisotropic smallness of a level of operator, one can define the anisotropy operator

$$\hat{K}^{\text{so}} = U_{xz}^\dagger V_x U_{xz} - V_z \quad (13)$$

and use this operator as a new perturbation (PT2 below). In this case the ground state Hamiltonian and wave function of the ground state are redefined to include a corresponding isotropic part of the SOC for each field direction. Strictly speaking, this approach is suitable only for magnetic insulators due to the dependence of the Fermi level on the direction of magnetic field. In metals it contains an uncontrolled error. It is expected, however, that this correction is small even in metals, and the expression above should be good enough for practical applications or an additional analysis of MAE.

But even in metals one can introduce a more rigorous form for the anisotropy operator. Let us turn from finite differences

to a transformation of the SOC operator V under an infinitesimal rotation. The operator V in a rotated coordinate system is related to the operator in an initial coordinate system by

$$V' = U(\omega, \Theta, \Phi)V[U(\omega, \Theta, \Phi)]^{-1}, \quad (14)$$

where U is a rotation operator and can be written as

$$U(\omega, \Theta, \Phi) = e^{-i\omega\mathbf{n}\cdot\mathbf{L}}, \quad (15)$$

where \mathbf{L} is the total orbital momentum operator.

Correspondingly, a transformation of the SOC operator V under an infinitesimal rotation has the form

$$V \rightarrow V' = V - i\delta\omega\mathbf{n} \cdot [\mathbf{L}, V]. \quad (16)$$

A corresponding operator of anisotropic torque (see also [16,17])

$$T^{\text{so}} = \frac{\delta V}{\delta\omega} = -i\mathbf{n} \cdot [\mathbf{L}, V]. \quad (17)$$

The angular variation extracted from the SOC energy is only a small anisotropic part, and the traditional variation over the inverse of the speed of light (PT1 below) allows us to obtain the sum of both small anisotropic and large isotropic SOC energies. After the application of the CCI formalism to matrix elements of this derivative, one can write the expectation value of the anisotropic part of the TE as

$$E'(\omega) = \langle \Psi(\omega) | T^{\text{so}} | \Psi(\omega) \rangle. \quad (18)$$

By integrating over all angles we obtain the total MAE. Below, this method will be called CCI2. Note that the Fermi energy and wave functions were determined for each angle and include the needed Fermi level change with magnetic field direction. Again, both definitions are suitable for the analyses of weak anisotropic interactions (<0.01 eV). Our goal now is to check how to correctly calculate the dependence of SOC energies on λ and ω and apply this to the MAE calculation in methods where the TE cannot be obtained with an accuracy of 0.001 meV.

In realistic material calculations, all approaches described above not only can serve as an alternative method for TE evaluations but also provide a way to decompose the TE ΔE into atomic components within different spin-orbital channels. Such component analysis will give more detailed insight on how SOC determines MAE in different materials.

Magnetocrystalline anisotropy

To discuss the meaning of SOC torque let us use the orbital moment anisotropy (OMA), defined as the difference between two self-consistently calculated orbital magnetic moments M_l for two different magnetic field directions, $M_l(0001) - M_l(\theta)$.

Yosida *et al.* [18] used the impurity Green's function approach and obtained several relations between different spin contributions to MAE and OMA. Since then, this approach has been used many times in different areas [19–22]. The most recent reviews of these methods can be found in Refs. [23–25]. Below we will use the original approach [18]. In the considered PT formalism the SOC energy is [18,19]

$$E_{\text{so}} = -\frac{\lambda}{2}(L_z^{\uparrow\uparrow} + L_z^{\downarrow\downarrow} + L_+^{\uparrow\downarrow} + L_-^{\downarrow\uparrow}), \quad (19)$$

where $L_i^{\sigma\sigma'}$ is the matrix element of the i th component of the orbital moment \hat{l}_i between corresponding spin states. The total relativistic energy of the system is a sum of SOC energy and a corresponding relativistic response of kinetic and potential energies. Using Eq. (10) for the energy change, we have

$$E = -\frac{\lambda}{4}(L_z^{\uparrow\uparrow} + L_z^{\downarrow\downarrow} + L_+^{\uparrow\downarrow} + L_-^{\downarrow\uparrow}). \quad (20)$$

The total orbital moment is defined as

$$M_l = M_l^{\uparrow\uparrow} + M_l^{\downarrow\downarrow} = -L_z^{\uparrow\uparrow} + L_z^{\downarrow\downarrow}. \quad (21)$$

The negative sign for the spin-up component appears explicitly only when PT is used, while in the fully relativistic Dirac approach all spin components formally have the same sign. For spin longitudinal components of the TE we can write

$$E^{\sigma\sigma} = \sigma_z \frac{\lambda}{4} M_l^{\sigma\sigma}, \quad (22)$$

where $\sigma_z = 1(-1)$ for $\sigma = \uparrow(\downarrow)$.

Despite all of the approximations used, recent calculations in many metallic systems with a very different strength of the SOC showed [8] that this expression is still fulfilled in realistic systems with a possible error of just 5%–10%. It seems that this approach as a whole can be used for the analysis of relativistic energies on a scale of typical SOC energies (0.05–0.5 eV).

A similar relation between different spin longitudinal components of MAE and OMA holds,

$$K^{\sigma\sigma} = -\sigma_z \frac{\lambda}{4} \Delta L_z^{\sigma\sigma}, \quad (23)$$

emphasizing that an easy magnetization axis direction for each spin component separately corresponds to a larger orbital moment for the same spin component (which is also just a Hund's rule statement for each spin component). While it is valid for each spin component separately, there is no such relation between the total MAE and the total OMA due to the presence of the negative sign in Eq. (21) for the spin-up component [23,24]. Such importance of the OMA is related to the fact that the spin moment anisotropy is very tiny, while a change in orbital moment is normally at least 5–10 times larger. This angular dependence of the amplitude (or spin projection) of the orbital magnetic moment is of fundamental importance as it provides a dominating contribution to both symmetric and antisymmetric anisotropic couplings between magnetic moments in magnets. However, the high-order small anisotropy of the spin moment can still be relevant, for instance, in the context of anisotropic magnetoresistance.

The total MAE in the case of half-metallic magnetism coincides with the total relativistic energy of spin-down states and can be presented as [18,24]

$$K = K^{\downarrow\downarrow} = \frac{\lambda}{4} L_z^{\downarrow\downarrow} = \frac{m^2}{4} \lambda^2 N_m^{\downarrow}(E_F) \quad (24)$$

Clearly, the PT relation for the orbital moment $L^{\downarrow\downarrow} = m^2 N_m^{\downarrow}$ will be strongly violated in the case of a very narrow peak when the value of $L^{\downarrow\downarrow}$ is unphysically large. In this case, while λ for 3d atoms is much smaller than the crystal field splittings, it can be comparable to the bandwidths of xy and $x^2 - y^2$ narrow peaks at E_f , and PT is no longer valid. The real typical

example will be an atom ($N_m^\downarrow \rightarrow \infty$) where $L^{\downarrow\downarrow}$ has limited and integer values of 0, 1, 2, To obtain a proper description of the orbital moment in this limit one has to go beyond the second order of the traditional Rayleigh-Schrodinger PT, as it does not describe the orbital moment properly [26]. A different version of the PT, namely, the Brillouin-Wigner PT [27], allows us to resolve this issue already in the second order. In the Brillouin-Wigner approach the relativistic modification of the DOS N_m^\downarrow can be presented as $N/\sqrt{1+m^2\lambda^2N^2}$, so the orbital moment for the down-spin component is

$$L^{\downarrow\downarrow} = m \frac{m\lambda N_m^\downarrow}{\sqrt{1+(m\lambda N_m^\downarrow)^2}}, \quad (25)$$

so in the atomic limit

$$L^{\downarrow\downarrow} = \lim_{N_m^\downarrow \rightarrow \infty} \left(m \frac{m\lambda N_m^\downarrow}{\sqrt{1+(m\lambda N_m^\downarrow)^2}} \right) = m, \quad (26)$$

and, for instance, for degenerate $x^2 - y^2$ and xy orbitals at E_f it will equal 2 for any value of λ , while for the specific nonrelativistic case of $\lambda = 0$, $L^{\downarrow\downarrow} = 0$. Thus, accounting for a proper relativistic modification of the effective bandwidth for systems with a large DOS at E_f can be crucial. Typically, the SOC in $3d$ atoms is around 0.05 eV; therefore, for the orbital moment $M_l = 2\mu_B$ one can expect that the theoretical maximum of the MAE can reach the huge value of 25 meV. An even higher value can be seen for highly localized $4f$ orbitals at the Fermi level.

Let us summarize all conditions of such a half-metallic model of a large magnetic anisotropy system. All spin-up states should be far from E_f . Such situation corresponds to the effective spin splitting being much larger than a characteristic SOC. A spin splitting of 1 eV would be already sufficient. Next, crystal field splitting separating states at E_f and all other d states with the same spin should be at least as large as the exchange splitting. This is exactly a case of strongly correlated narrow-bandwidth electronic materials where such methods as DMFT should be used. Such PT estimations are not suitable for majority of $4f$ -electron-based magnetic systems where the SOC cannot be considered as a perturbation, and a full relativistic treatment is needed. In such cases the contribution to the MAE from SOC alone can be rather small and have a different sign. While the relativistic PT is not applicable here, the CCI methods proposed above can be used to analyze the relativistic interactions.

III. RESULTS AND DISCUSSION

In this section, we numerically benchmark the accuracy of CCI in evaluating the TE change ΔE and the MAE due to SOC.

A. TE ΔE from CCI

To investigate the reliability of the CCI given in Eq. (6), we carry out all-electron first-principles DFT calculations using the full potential relativistic linearized augmented plane-wave package (WIEN2K) [28]. Three single-element fcc crystals, Al, Pt, and Pu, which have increasing SOC strength, are chosen

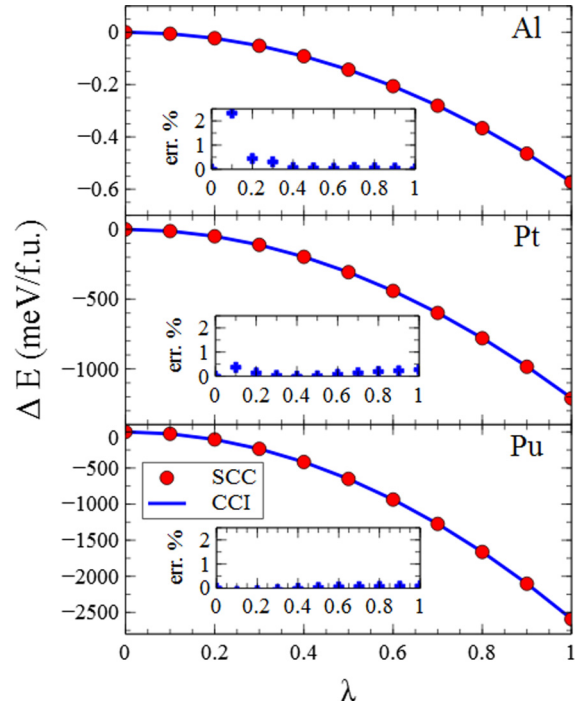


FIG. 1. TE change ΔE due to SOC as a function of coupling constant λ calculated with SCC and the CCI method. CCI energies agree very well with SCC results for fcc crystals Al (top), Pt (middle), and Pu (bottom).

for the benchmark. The lattice constants are 7.653, 7.417, and 8.754 bohrs, respectively. The self-consistent calculations are done with a $21 \times 21 \times 21$ uniform k -point mesh. The LDA is adopted for the exchange-correlation functional. The Fermi broadening method with a broadening factor of 0.002 Ry is used for the Brillouin zone k -point summation. The TE tolerance is set to 10^{-8} Ry to guarantee the convergence of the self-consistent calculations.

Figure 1 shows the TE change $\Delta E(\lambda)$ due to SOC as a function of coupling constant λ from SCCs (red dots) and CCI calculations (blue curve). One can see that the CCI data agree very well with the numerically exact SCC results in the range of SOC strength across three orders of magnitude from Al to Pu. The relative error, defined as $(\Delta E_{CCI} - \Delta E_{SCC})/\Delta E_{SCC}$, is generally less than 1%, as shown in the insets of Fig. 1. In particular, Table I lists relative errors for $\lambda = 1$, which corresponds to the physical SOC in real materials. The relative errors are smaller than half a percent, indicating that CCI is a reliable approach for TE calculations.

TABLE I. Comparisons of the TE change ΔE due to SOC, obtained from CCI calculations and SCCs. The relative errors are less than half a percent.

	Al	Pt	Pu
ΔE_{SCC} (meV/f.u.)	-0.5725	-1211.84	-2591.67
ΔE_{CCI} (meV/f.u.)	-0.5724	-1208.57	-2594.06
Error (%)	0.016	0.270	0.092

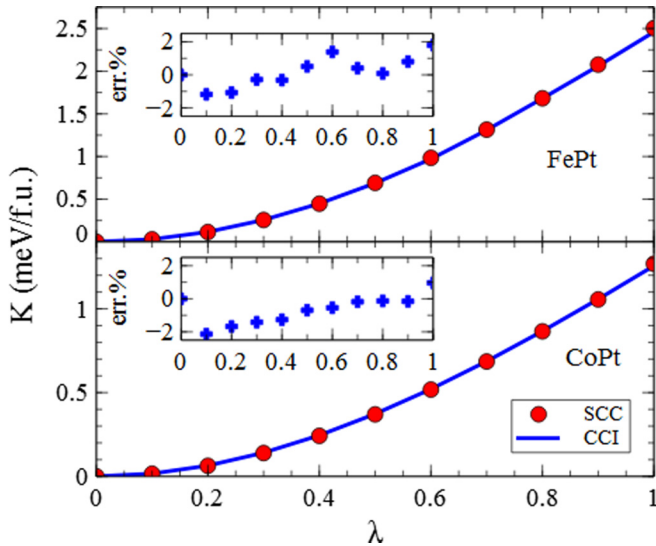


FIG. 2. Magnetic anisotropy energy K of FePt and CoPt as a function of the coupling constant λ calculated from SCC and the CCI method. The CCI method is shown to be able to generate results in close agreement with the numerically precise SCC.

B. MAE from CCI

We further investigate the reliability of CCI in determining MAE, which is a very important property for permanent magnets and also much more challenging to calculate since it is usually very small. Two typical examples of ferromagnetic materials with high MAE are FePt and CoPt, with $L1_0$ structure. We took experimental values as lattice constants: $a = 5.218$ bohrs, $c = 7.058$ bohrs for FePt and $a = 5.070$ bohrs, $c = 6.970$ bohrs for CoPt [29]. The MAE here calculated amounts to the difference of two magnetization orientations, [100] and [001] (the [001] axis is perpendicular to the alternating Fe/Co and Pt planes). In order to reduce the numerical errors, we use the same (lower) space symmetry group for two orientations and a common $40 \times 40 \times 29$ k -point mesh. Even though FePt and CoPt both exhibit large MAE compared to other materials, the scale is still just around meV—much smaller than TE. In Fig. 2 we show MAE as a function of the coupling constant λ from SCC and the CCI method. The CCI produces results in very good agreement with SCCs for both structures. The relative error is generally smaller than 2%, as shown in the insets of Fig. 2. Our calculation results also agree fairly well with the early calculations in the literature [7,24].

For a more detailed study of the efficiency and accuracy of the CCI method, we investigate the CCI results given different numbers of sampling λ points. Table II presents the results using three, five, and ten λ points (including the trivial point at $\lambda = 0$) uniformly sampled between 0 and 1. The errors are consistently fairly small even with a small number of sampling points.

C. Site decomposition based on CCI

Seeing that the SOC is purely local interactions, the CCI method provides a feasible way to decompose the TE variation ΔE due to the response to SOC, including MAE, into atomic site (and spin-orbital) components. Such site decomposition

TABLE II. Comparisons of the MAEs for FePt and CoPt calculated from SCCs and the CCI method. The relative errors are shown to be very small.

	FePt	CoPt
E_{SCC} (meV/f.u.)	2.505	1.269
E_{CCI}^a (meV/f.u.)		
Three points	2.426 (3.1%)	1.264 (0.4%)
Five points	2.429 (3.0%)	1.258 (0.9%)
Ten points	2.474 (1.2%)	1.257 (0.9%)

^aThe error is shown in parentheses.

is complete; that is, the sum of all energy site components is exactly equal to the TE. No interstitial regions are involved. Valuable information about the role of different sites (including spin-orbital channels) in the response to the SOC and the microscopic origin of the system MAE can be obtained. Such information can be used to guide material design and optimization, for instance, through chemical substitution.

Figure 3 presents the TE change ΔE (left panel) and MAE (right panel) in terms of Fe/Co site and Pt site components for FePt and CoPt alloys. The Pt site obviously plays the dominant role in the TE change induced by SOC because of its larger mass. Interestingly, such site-component analysis reveals that the major contribution for the large MAE of these materials comes from Pt site, rather than Fe/Co site. Even more remarkably, the Fe/Co site is found to have a negative contribution to the material MAE. The analysis suggests that Fe/Co site chemical substitution might be used to further improve the MAE of this type of materials.

D. DMFT calculations

We calculate the electronic structure within DFT+SOC+DMFT using the full potential implementation and the TRIQS library [30]. In the DFT part of the computation, the WIEN2K package was used with the gradient correction approximation. For projectors on the correlated orbital in DFT+DMFT, Wannier-like orbitals are constructed out of Kohn-Sham bands within the energy window from -2 to 1 eV with respect to the Fermi energy. This window is also

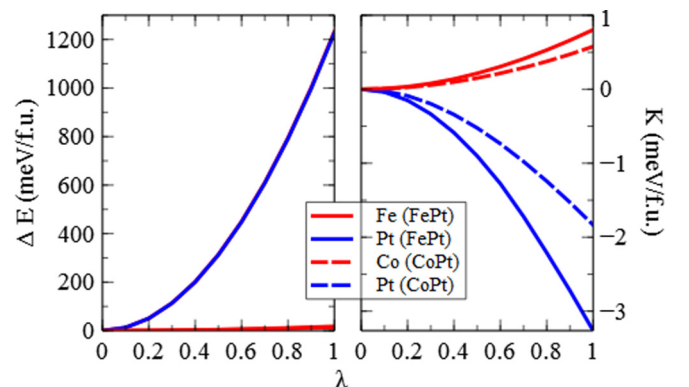


FIG. 3. CCI-based site components of the TE change ΔE and MAE. The Pt site clearly dominates the contribution to ΔE (due to SOC) and MAE of the two materials.

TABLE III. The MAE obtained using both PT schemes and CCI methods described in the text for different magnetic systems. Calculations using VASP with the GGA performed for Co and CoPt and LDA+ U for CoO are shown in comparison with the corresponding DMFT calculations. Experimental lattice constants have been used. All values for hcp Co are in $\mu\text{eV}/\text{atom}$; other values are in meV/cell .

	Co (hcp)		CoPt		YCo ₅		CoO	
	GGA	DMFT	GGA	DMFT	GGA	DMFT	GGA+ U	DMFT
PT1	24.5	46	1.152	1.31	1.715	3.35	1.44	1.70
PT2	22.3	46	1.105	1.32	1.760	3.39	1.43	1.71
CCI1	28.5	49	1.217	1.38	1.904	3.44	1.42	1.72
CCI2	27.5	50	1.223	1.39	1.951	3.49	1.44	1.73
TE	29.1		1.241		1.926		1.42	1.72

suitable for the correct treatment of the SOC operator, while for the anisotropy operator an even smaller energy range is sufficient. To solve the DMFT quantum impurity problem, we used the strong-coupling continuous-time Monte Carlo impurity solver as implemented in the TRIQS library with the off-diagonal hybridization elements included.

The U and J parameters for Co atoms have been used according to the suggestions of Ref. [8].

Our results are presented in Table III. The usual TE DFT calculations of the MAE for hcp Co have been performed for many years, and these results differ greatly but are consistently far from the experimental number ($64 \mu\text{eV}/\text{atom}$). Our GGA result ($29 \mu\text{eV}/\text{atom}$) confirms this trend. While for CoPt GGA gives satisfactory agreement with the experimental number (see Table III), for YCo₅, again, our and published earlier data indicate a significant deviation from the experiment. Note that for Co and YCo₅ different density functional studies demonstrated that the results are sensitive to the quality of calculations and the choice of the exchange correlation potential.

Overall, our calculations of perturbation energies and the results of corresponding CCI methods show very similar trends in metals. The relativistic second-order PT1 and its anisotropic analog PT2 produced the worst (but still satisfactory) agreement with the corresponding number obtained from TE calculations, with a typical deviation $<20\%$. The PT2 scheme gives a bit larger disagreement, which we associate with a shift in the Fermi level. Both CCI schemes produced much better agreement with the corresponding TE result ($1\%–5\%$) in all studied metals. In the magnetic insulator CoO the difference between the PT and CCI methods is very small and probably related only to the accuracy of the different numerical methods. We do not show GGA results for CoO as it produced the wrong ground state. In this case we switched to the GGA+ U scheme.

Our DMFT studies confirm a general trend between PT and CCI methods, showing a clear difference between their results. While for CoPt DMFT produced a result similar to the GGA for MAE in all tested methods, for Co and YCo₅ DMFT results are very different from those obtained with the GGA, demonstrating an increase in MAE of nearly a factor of 2. In turn DMFT greatly improves the agreement with the measured numbers for both systems. For YCo₅, such influence

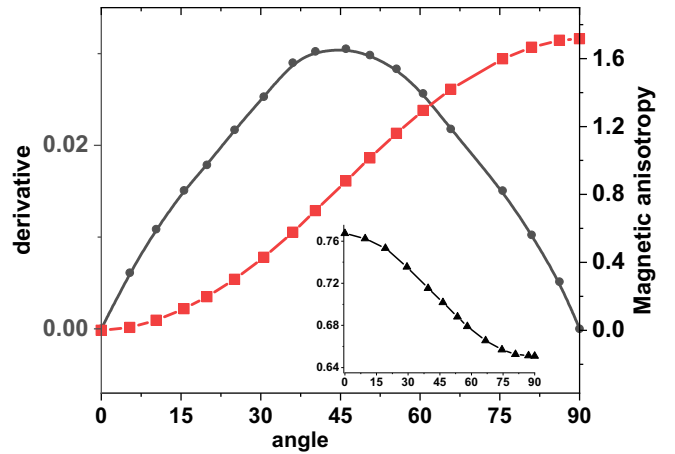


FIG. 4. The angular dependence of magnetic anisotropy (right, in meV) and anisotropic torque (left) in CoO as a function the magnetic field angle ($\phi = 90$). Inset: the orbital moment on Co atom (in units of μ_B).

of correlation effects was noticed before [8], while for hcp Co, to our knowledge, it has not been discussed.

Let us describe the equilibrium magnetic moments in these systems. In hcp Co the obtained DMFT total magnetic moment $M_t = M_s + M_l$ is $1.69\mu_B = 1.57\mu_B + 0.14\mu_B$, which traditionally is very close to the experimental $1.66\mu_B$ ($1.52\mu_B + 0.14\mu_B$). The DMFT spin (orbital) moment of the Co atom in CoPt is unusually large, $2.08\mu_B$ ($0.28\mu_B$). However, the OMA is rather weak, and overall, the Co atom practically does not contribute to the total MAE. The M_l of the Pt atom ($0.1\mu_B$) in turn is very anisotropic with a very unusual structure [24], so the Pt atom produces the dominating contribution to the MAE of CoPt.

The interesting feature of YCo₅ is the difference between orbital moments on the 2c and 3g sites of Co [19], which has been well established experimentally. This difference is usually associated with the observed large MAE in YCo₅. Our DMFT calculations give $M_l = 0.29\mu_B$ (2c) and $M_l = 0.19\mu_B$ (3g site) with dominating orbital moment anisotropy on the 2c sites. Similar results were obtained in DMFT and LDA+ U calculations previously [8,9].

In the magnetic insulator CoO the PT and CCI results are expected to be similar, and our DMFT applications confirmed it. We also used the TE calculations of DMFT to compare all schemes. In such insulating systems the MAE obtained from the TE is not as sensitive to the computational details as in metals. However, it is still hard to achieve consistently an accuracy of 0.1 meV or less due to DMFT features, including the natural stochastic origin of numerical many-body methods. The results of anisotropy calculations from TE in DMFT have better accuracy due to some error cancellation effects when calculating the difference between two large numbers. A similar accuracy ($<1 \text{ meV}$) was reported earlier for DMFT calculations [9].

Finally, in Fig. 4 we show the anisotropy and anisotropic torque (see above) for AFM CoO ($\phi = 90$) as a function of the magnetic field angle. It is well known that for this system LDA (GGA) produces a metallic ground state, while the addition

of Hubbard's U (4 eV in our case) leads to a gap opening, in agreement with the experiment. In addition, several possible easy-axis directions were proposed by the experiments [31–33]. Our results support the oldest findings [31]. The total magnetic moment in CoO is $3.52\mu_B$ ($2.75\mu_B + 0.77\mu_B$) and looks somewhat smaller than the measured values [31–33]. A larger orbital moment in Co ($1\mu_B$) was found a long time ago in LDA+ U calculations in Ref. [34]. We relate this difference to the significantly larger Hubbard parameter used there.

IV. CONCLUSIONS

We performed a numerical investigation of the reliability of different perturbation theory and coupling constant integration methods for evaluating the TE change induced by SOC. The magnetocrystalline anisotropy, a technologically very important physical property for permanent magnets, was also included as a more stringent test. All methods showed consistently good agreement with the numerically precise total energy results from well-converged self-consistent calculations within the theoretical framework of DFT, on energy scales across several orders of magnitude and different materials. Therefore, all considered methods are expected to be reliable and useful, especially for similar calculations within other theoretical frameworks where an accurate TE is hard

to obtain like DMFT and GW methods. Both PT and CCI methods offer a reasonable accuracy for much smaller computational efforts. These methods also offer a practical way to decompose the induced TE variation into different sites and spin-orbit components. They can be used as a more justified approximation relative to the popular one-electron analysis. PT/CCI energy component analysis provides a feasible way to obtain intuitive understanding of how systems respond in the presence of SOC, especially the microscopic origin of MAE, which can serve as theoretical guidance for material design and optimization.

ACKNOWLEDGMENTS

V.P.A. is grateful to L. Benedict for helpful discussions and to A. Lichtenstein and members of his group at Hamburg University for numerous discussions of the DMFT method. This work is supported by the US Department of Energy (DOE), Office of Science, Basic Energy Sciences, Materials Science and Engineering Division, including the grant of computer time at the National Energy Research Scientific Computing Center (NERSC) in Berkeley, California. The research was performed at Ames Laboratory, which is operated for the US DOE by Iowa State University under Contract No. DE-AC02-07CH11358.

-
- [1] V. N. Antonov and V. P. Antropov, *Low. Temp. Phys.* **46**, 1 (2020).
 - [2] V. I. Anisimov, J. Zaanen, and O. K. Andersen, *Phys. Rev. B* **44**, 943 (1991).
 - [3] V. I. Anisimov, F. Aryasetiawan, and I. Lichtenstein, *J. Phys.: Condens. Matter* **9**, 767 (1997).
 - [4] A. Georges, G. Kotliar, W. Krauth, and M. J. Rozenberg, *Rev. Mod. Phys.* **68**, 13 (1996).
 - [5] G. Kotliar, S. Y. Savrasov, K. Haule, V. S. Oudovenko, O. Parcollet, and C. A. Marianetti, *Rev. Mod. Phys.* **78**, 865 (2006).
 - [6] I. Yang, S. Y. Savrasov, and G. Kotliar, *Phys. Rev. Lett.* **87**, 216405 (2001).
 - [7] A. B. Shick and O. N. Mryasov, *Phys. Rev. B* **67**, 172407 (2003).
 - [8] M. C. Nguyen, Y. Yao, C.-Z. Wang, K.-M. Ho, and V. P. Antropov, *J. Phys.: Condens. Matter* **30**, 195801 (2018).
 - [9] J.-X. Zhu, M. Janoschek, R. Rosenberg, F. Ronning, J. D. Thompson, M. A. Torrez, E. D. Bauer, and C. D. Batista, *Phys. Rev. X* **4**, 021027 (2014).
 - [10] L. V. Pourovskii, J. Boust, R. Ballou, G. G. Eslava, and D. Givord, *Phys. Rev. B* **101**, 214433 (2020).
 - [11] L. Hedin, *Phys. Rev.* **139**, A796 (1965).
 - [12] F. Aryasetiawan and O. Gunnarsson, *Rep. Prog. Phys.* **61**, 237 (1998).
 - [13] M. van Schilfgaarde, T. Kotani, and S. Faleev, *Phys. Rev. Lett.* **96**, 226402 (2006).
 - [14] A. Görling and A. Heilmann, *Mol. Phys.* **109**, 2473 (2011).
 - [15] Y. Sun, Y.-X. Yao, M. C. Nguyen, C.-Z. Wang, K.-M. Ho, and V. Antropov, *Phys. Rev. B* **102**, 134429 (2020).
 - [16] V. P. Antropov and A. I. Liechtenstein, *Mater. Res. Soc. Symp. Proc.* **253**, 325 (1991).
 - [17] X. Wang, R. Wu, D. S. Wang, and A. J. Freeman, *Phys. Rev. B* **54**, 61 (1996).
 - [18] K. Yosida, A. Okiji, and S. Chikazumi, *Prog. Theor. Phys.* **33**, 559 (1965).
 - [19] R. L. Streever, *Phys. Rev. B* **19**, 2704 (1979).
 - [20] I. V. Solov'yev, P. H. Dederichs, and I. Mertig, *Phys. Rev. B* **52**, 13419 (1995).
 - [21] J. Inoue, *J. Phys. D* **48**, 445005 (2015).
 - [22] M. Cinal, D. M. Edwards, and J. Mathon, *Phys. Rev. B* **50**, 3754 (1994).
 - [23] G. van der Laan, *J. Phys.: Condens. Matter* **10**, 3239 (1998).
 - [24] V. Antropov, L. Ke, and D. Åberg, *Solid State Commun.* **194**, 35 (2014).
 - [25] J. Stöhr and H. Siegmann, in *Magnetism: From Fundamentals to Nanoscale Dynamics* (Springer, Berlin, 2006), p. 805.
 - [26] V. P. Antropov and V. N. Antonov, *Phys. Rev. B* **90**, 094406 (2014).
 - [27] I. Hubac and S. Wilson, *J. Phys. B* **33**, 365 (2000).
 - [28] P. Blaha, K. Schwarz, G. K. H. Madsen, D. Kvasnicka, and J. Luitz, *WIEN2K: An Augmented Plane Wave+ Local Orbitals Program for Calculating Crystal Properties* (Technische Universität Wien, Vienna, 2001).
 - [29] K. Buschow, P. van Engen, and R. Jongebreur, *J. Magn. Magn. Mater.* **38**, 1 (1983).
 - [30] M. Aichhorn, L. Pourovskii, P. Seth, V. Vildosola, M. Zingl, O. E. Peil, X. Deng, J. Marvlje, G. Kraberger, C. Martins, M. Ferrero, and O. Raccollet, *Comput. Phys. Commun.* **204**, 200 (2016).
 - [31] W. L. Roth, *Phys. Rev.* **110**, 1333 (1958).
 - [32] D. Herrmann-Ronzaud, P. Burlet, and J. Rossat-Mignod, *J. Phys. C* **11**, 2123 (1978).
 - [33] W. Jauch, M. Reehuis, H. J. Bleif, F. Kubanek, and P. Pattison, *Phys. Rev. B* **64**, 052102 (2001).
 - [34] I. V. Solov'yev, A. I. Liechtenstein, and K. Terakura, *Phys. Rev. Lett.* **80**, 5758 (1998).